Study on protein conformation and adsorption behaviors in nanodiamond particle–protein complexes

2011 Nanotechnology 22 145703

(http://iopscience.iop.org/0957-4484/22/14/145703)

Nanotechnology **22** (2011) 145703 (10pp) doi:10.1088/0957-4484/22/14/145703

Study on protein conformation and adsorption behaviors in nanodiamond particle–protein complexes

Hai-Dong Wang[1], Catherine Hui Niu[2,5], Qiaoqin Yang[3] and Ildiko Badea[4]

[1] Department of Biomedical Engineering, University of Saskatchewan, Saskatoon, S7N 5A9, Canada
[2] Department of Chemical Engineering, University of Saskatchewan, Saskatoon, S7N 5A9, Canada
[3] Department of Mechanical Engineering, University of Saskatchewan, Saskatoon, S7N 5A9, Canada
[4] Drug Design and Discovery Research Group, College of Pharmacy and Nutrition, University of Saskatchewan, Saskatoon, S7N 5C9, Canada

E-mail: catherine.niu@usask.ca

Received 7 December 2010
Published 24 February 2011
Online at stacks.iop.org/Nano/22/145703

Abstract

In the present research, the conformation of bovine serum albumin (BSA) in the nanodiamond particle (ND)–BSA complex was studied by Fourier transform infrared spectroscopy, fluorescence spectroscopy, UV–vis spectroscopy, and circular dichroism spectroscopy. The spectroscopic study revealed that most BSA structural features could be preserved in the complex though the BSA underwent conformational changes in the complex due to ND–BSA interaction. In addition, BSA adsorption isotherms and zeta-potential measurements were employed to investigate the pH dependence of the ND–BSA interaction. The changes in surface charge of the ND–BSA complex with pH variations indicated that the binding of BSA to ND might lead to not only the adsorption of BSA onto the ND surface but also the partial breakup of ND aggregates into relatively small ND–BSA aggregates because of the strong binding force between ND and BSA. The results show that ND is an excellent platform for protein immobilization with high affinity and holds great potential to be used for biosensor applications.

1. Introduction

Nanotechnology has been undergoing rapidly exploding development in recent years which could find wide applications in a broad range of scientific areas [1–3]. The combination of nanotechnology and biotechnology gives rise to a newly emerging interdisciplinary field: nanobiotechnology [4]. Nanobiotechnology, which incorporates the unique properties of biomolecules (recognition, transport, and catalytic properties, etc) with those of nanoparticles (electronic, photonic, and catalytic properties, etc), is playing an increasingly important role in biomedical engineering [4]. Nanodiamond particles (NDs) have recently come into the focus as a new promising nanomaterial due to their exceptional properties including high specific surface area and the concomitant high adsorption capability, oxygen-containing functional groups on the surface, optical transparency, and highly chemically inert sp^3 carbon (diamond) cores [5–7]. By virtue of their chemical and physical inertness, NDs have excellent biocompatibility which has already been proved by many previous studies [5, 8, 9]. The research on the cytotoxicity of NDs revealed that NDs have no cytotoxicity to cells while other carbon nanomaterials such as carbon nanotube and C60 exhibit cytotoxicity to different extents based on previous reports [10, 11]. All these properties endow NDs with novel and promising biotechnological applications [12].

Biomolecules have been immobilized on nanoparticles through a variety of techniques including covalent coupling

[5] Author to whom any correspondence should be addressed.

and physical adsorption by noncovalent interaction such as hydrophobic interaction, electrostatic binding, and specific recognition [4]. The noncovalent method is especially applicable to NDs whose surfaces could be terminated with carboxyl groups or other oxygen-containing groups for the interaction with the amino groups of proteins [13]. According to the previous research, NDs show high affinity with biomolecules such as proteins [12–16], enzymes [17, 18], antibodies [19] and peptides [20], which indicates that a ND is an exceptional platform for biomolecule adsorption and immobilization [13]. This property makes NDs promising for many biological applications including biosensors [19] and diagnostic tools in clinical proteomics research [12]. However, the strong interaction between NDs and biomolecules may cause structural changes of the biomolecules [21, 22]. In order to understand the protein adsorption mechanism and identify the optimal conditions to preserve the functionality of protein following protein immobilization on NDs, it is necessary to investigate the conformation of protein upon binding with NDs [21, 23]. But there has been no systematic investigation in this regard so far [13].

BSA is a well-characterized protein, which is a so called 'soft' protein with low internal stability and therefore could easily undergo conformational changes upon environment changes [24]. In the present work, BSA was chosen as a model protein for the study of protein conformation and the interaction between NDs and protein in their complex. The results have demonstrated that an ND is an excellent platform for protein immobilization with high affinity and most of the BSA structural features could be preserved upon immobilization, suggesting that NDs hold great potential for biosensor applications.

2. Materials and methods

2.1. Materials

Detonation NDs, which have an average particle size of 3–5 nm, were purchased from Nanostructured and Amorphous Materials Inc. and used without further treatment. Bovine serum albumin (BSA), purchased from Bio Basic (purity > 98%), was used as received. All other reagents were of analytical grade and used without further purification. The water used in the present research was from a milli-Q system.

2.2. Fourier transform infrared (FT-IR) studies

To investigate the influence of ND–BSA interaction on the conformational changes of BSA in the ND–BSA complex, FT-IR spectra were recorded on a JASCO FT/IR-4100 spectrometer.

The ND–BSA complex was obtained by mixing an ND suspension (in pH 7.4 phosphate buffer, 0.1 M) and BSA solution (in pH 7.4 phosphate buffer, 0.1 M) and then separating the ND–BSA complex from the solution by centrifugation. The complex was repeatedly rinsed with milli-Q water to remove unbound BSA. The ND–BSA complex was lyophilized to dryness. 1 mg of the ND–BSA complex was then ground with 100 mg of dried KBr to form homogeneous powder. After that approximately 25 mg of the powder was made into pellets which were subjected to FT-IR measurement for absorbance spectrum. For each measurement, a total of 64 scans were averaged with a resolution of 4 cm^{-1}. This KBr-based method has been proved not to introduce artificial structural change to protein in previous analyses [25, 26]. For the measurement of the ND–BSA complex, a reference spectrum (an ND/KBr mixture possessing an identical amount of NDs to that in the ND–BSA complex) was recorded in an identical manner and subtracted from that of the ND–BSA complex. For BSA, the BSA/KBr powder used for the measurement had the same BSA content as that in the ND–BSA/KBr powder and pure KBr was employed as reference. The baselines of the spectra were corrected according to the criterion that a straight baseline was obtained in the region from 1750 to 2000 cm^{-1}, which is critical to obtain correct structural information using the second derivative analysis method [25, 27]. Second derivatives were then obtained using spectrum analysis software on a JASCO FT-IR spectrometer.

2.3. Ultraviolet–visible (UV–vis) absorption spectra

UV–vis spectra were recorded on a UV–vis spectrophotometer (Shimadzu UVmini-1240) with wavelength ranging from 240 to 310 nm. The contribution of light scattering from NDs was determined by plotting $\log_{10}$ (absorbance) as a function of $\log_{10}$ (wavelength) above 310 nm and then extrapolating linearly to shorter wavelengths, since BSA does not show absorbance at wavelength higher than ca. 310 nm [28]. Then the effect of light scattering from the NDs was removed from the UV–vis spectra. The BSA concentration was fixed at 1.5×10^{-6} M in both ND–BSA complex solutions (buffered at pH 7.4 by 10 mM phosphate buffer) where the ND concentrations were 1.5×10^{-7} and 4.5×10^{-7} M, respectively. The sample solutions were prepared at room temperature right before the experiment. Each spectrum presented was the average of three scans. All measurements were performed at 25 °C.

2.4. Circular dichroism (CD) spectroscopy

The circular dichroism (CD) spectra of BSA in the absence and presence of NDs were recorded on a PiStar-180 Spectrometer (Applied Photophysics Ltd, UK) at 25 °C. All CD spectra were collected in a wavelength range from 200 to 250 nm using a rectangular quartz cell with 10 mm path length. Each spectrum was measured in triplicate with the data presented being the average. The BSA concentration was fixed at 2.5×10^{-7} M with the ND concentration ranging from 2.5×10^{-9} to 10^{-8} M. CD backgrounds were corrected for each measurement. All samples were buffered at pH 7.4 by 10 mM phosphate buffer. The α-helix content of BSA is determined by equation (1) [29, 30]:

$$\%\alpha\text{-helix} = \frac{(-[\theta_{208}] - 4000)}{(33\,000 - 4000)} \times 100 \qquad (1)$$

where $[\theta_{208}]$ is the mean residue ellipticity at 208 nm in deg cm^2 $dmol^{-1}$.

2.5. Fluorescence quenching measurements

Fluorescence measurements were performed on a fluorescence spectrophotometer (Cary Eclipse, Varian) at 25 °C. All the emission spectra were collected at the excitation wavelength of 295 nm using 5 nm/10 nm (excitation/emission) slit widths and a rectangular quartz cell with 10 mm path length. Each spectrum presented was the average of at least three scans. To avoid the inner filter effects, highly diluted solutions ([BSA] = 1.5×10^{-6} M and [NDs] = 1.2×10^{-8} to 8.2×10^{-8} M) were used for all measurements. Fluorescence backgrounds were corrected for blank buffer solutions in each measurement.

2.6. Equilibrium adsorption of BSA onto the ND surface

The NDs were dispersed, with ultrasonic treatment (Branson 2510 Sonication Bath), in phosphate buffer solution (0.1 M) at a concentration of 2.0 mg ml^{-1}. After that 5 ml of ND suspension was mixed with 5 ml of BSA solution buffered at the same pH by phosphate buffer (0.1 M). The ND–BSA suspension was then mixed thoroughly with a Multitron Incubator Shaker at 25 °C and 180 rpm for 2 h, which was confirmed to be more than adequate to establish adsorption equilibrium under the conditions of the present research. Finally the suspension was subjected to centrifugation on a Beckman Coulter Allegra X-22R centrifuge (15 000 rpm, 30 min) and the BSA concentration in the supernatant was analyzed on a UV/vis spectrophotometer (Shimadzu UVmini-1240) at a wavelength of 280 nm. All the samples were run in duplicate with data presented being the average. A blank reference was used during the adsorption experiment to confirm that the influence of floating NDs in supernatant was negligible. The BSA uptake was determined by the concentration difference between the initial BSA solution and the final supernatant, as expressed in equation (2):

$$q = \frac{(C_0 - C)V}{m} \tag{2}$$

where q is BSA uptake (mg g^{-1} dry NDs), C_0 and C are BSA concentrations in initial solution (mg ml^{-1}) and final supernatant (mg ml^{-1}), respectively. V is the solution volume (ml) and m the dry net weight of NDs (g).

2.7. Zeta-potential measurements

Zeta-potential measurements were carried out on a Zetasizer Nano ZS instrument (Malvern) over a pH range from approximately 9.0 to 3.0 at 25 °C. The zeta-potential was determined by measuring the electrophoretic velocity of the nanoparticles by a laser Doppler velocimetry technique. The pH of the solution measured was adjusted by an autotitrator using NaOH and HCl solutions. After reaching the desired pH by titration, the solution was left to equilibrate for 1 min before taking measurements. Each measurement was performed in triplicate with the data presented being the average. For all measurements, the ND concentration was fixed at 0.005 mg ml^{-1}. The BSA concentrations in the ND–BSA complex solutions were 0.001 25 and 0.005 mg ml^{-1}, respectively. The samples were prepared at room temperature right before the measurements. For the ND–BSA samples no centrifugation was used in order to retain the original conformation of BSA in complex.

3. Results and discussion

3.1. FT-IR characterizations

FT-IR spectroscopy is a widely used technique to study protein conformation [31–33]. Different amide bond orientations within peptide backbone can be attributable to various secondary structures such as α-helix, β-sheets, β-turns, and unordered structures (or referred to as random coil) [30, 34]. Among all amide bands (amide I, II, and III), amide I region (1600–1700 cm^{-1}, mainly due to C=O stretching vibration) has been proved to be helpful for protein conformational studies since it is the most sensitive to protein secondary structure changes [30]. According to previous research [25, 30, 31, 34–36], the assignment of secondary structures is as follows: 1695–1663 cm^{-1} for β-sheet or β-turn structures, 1662–1650 cm^{-1} for α-helices, 1648–1644 cm^{-1} for random chains, 1642–1618 cm^{-1} for β-sheets. Bands at lower wavenumbers (ca. 1616 cm^{-1}) have been assigned to side chain moieties.

The FT-IR spectra of native BSA as well as BSA in the ND–BSA complex are given in figure 1(a), where the amide I and II bands are shown. From figure 1(a) both native BSA and BSA in the ND–BSA complex show noticeable peptide bonds indicating that BSA has been attached onto the ND surface. Figure 1(b) further shows the specific difference in secondary structures by comparing second derivative spectra of native BSA and BSA in the ND–BSA complex. For native BSA, the α-helix dominates the spectra at ca. 1660 cm^{-1} which is also true for the ND–BSA complex where α-helix appears at ca. 1658 cm^{-1}. The intensity of unordered structure (ca. 1649 cm^{-1}) is higher in the complex than that in the native BSA. The intensities for β-turn (1694 and 1676 cm^{-1}) and β-sheet (1636 cm^{-1}) structures in native BSA are also found to increase in the ND–BSA complex. For most peaks, the peak position changes slightly after the formation of the complex. Moreover, a new peak at ca. 1629 cm^{-1}, which could be assigned to β-sheet structure, appears in the complex. All these changes in the BSA second derivative spectra indicate the strong interaction between NDs and BSA.

3.2. UV–vis and CD spectroscopies

UV–vis spectroscopy could provide information regarding whether major structural change occurred in proteins. The absorbance of protein in the 230–300 nm range is mainly attributable to aromatic residues, including tryptophan, tyrosine, and phenylalanine. The absorption spectra of the aromatic residues depend on their molecular environment which could give rise to the change in wavelength and intensity. In general, the shift in wavelength predominates. An evident blue-shift in the spectrum is likely to occur if the aromatic residue is exposed to an environment with more polarity. In the present work, as shown in figure 2, BSA absorption spectra at ca. 278 nm (aromatic residue) have nearly no shift upon

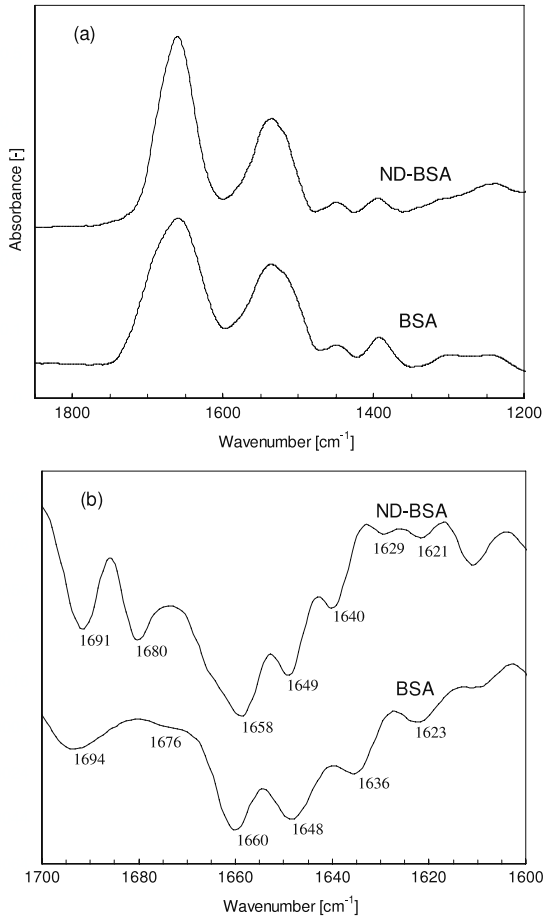

Figure 1. FT-IR spectra of (a) native BSA and BSA in the ND–BSA complex as well as (b) the corresponding second derivative spectra in the amide I region.

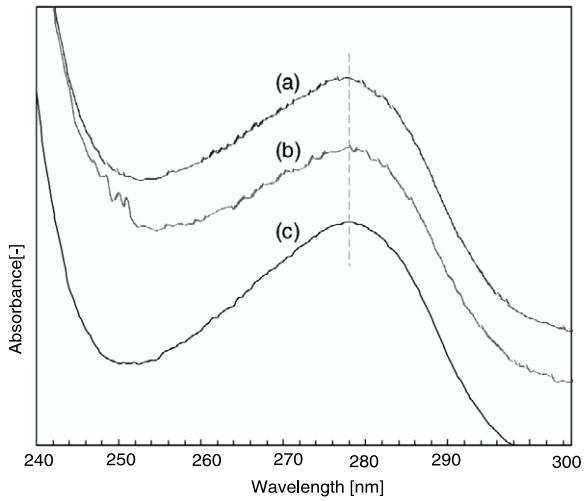

Figure 2. UV–vis absorption spectra of (a) BSA in the ND–BSA complex (ND concentration: 1.5×10^{-7} M), (b) BSA in the ND–BSA complex (ND concentration: 4.5×10^{-7} M), and (c) native BSA. The BSA concentration is fixed at 1.5×10^{-6} M.

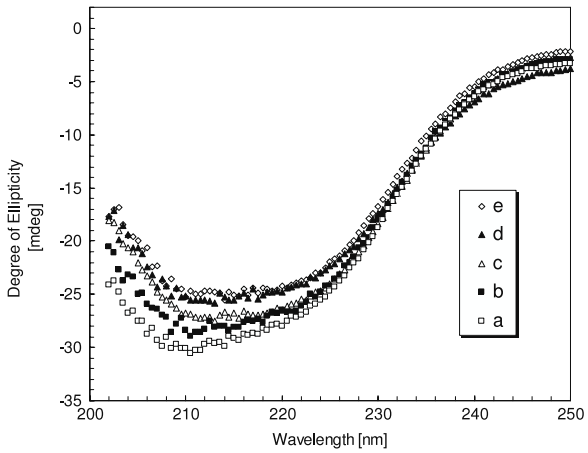

Figure 3. The CD spectra of 2.5×10^{-7} M BSA (curve a) with the regular addition of NDs at pH 7.4. The ND concentration is from 2.5×10^{-9} to 10^{-8} M (curves b–e).

forming a complex with NDs indicating that the formation of the ND–BSA complex might not result in major BSA unfolding.

For a quantitative analysis of to what extent BSA structural features could be preserved upon binding to the ND surface, CD spectroscopy is used to further study BSA conformation and conformational changes. The protein structural features determine its biological functionality so the study on CD spectra of protein could shed light on whether protein could retain its biological functionality. For albumin, which features a dominant content of α-helix in its secondary structure, α-helix content is actually a good indicator of its structural features, and a major loss of α-helix content probably suggests the loss of protein biological functionality [37, 38]. In CD spectroscopy, the α-helix features negative CD signals at 208 and 222 nm.

The CD spectra of native BSA in the absence or presence of NDs are given in figure 3. According to figure 3, native BSA at pH 7.4 (buffered by 10 mM phosphate buffer solution) has an α-helix content of ca. 55% which is consistent with the previous report [34]. With the regular addition of ND suspension (buffered at pH 7.4 by 10 mM phosphate buffer solution), the ellipticities of BSA at both 208 and 222 nm are gradually decreased indicating loss of BSA secondary structure upon forming a complex with NDs. However, BSA still has an α-helix content of ca. 43% (nearly 80% of its original α-helix content) even when the ND concentration is increased up to 10^{-8} M. Obviously most of the α-helix content in BSA is preserved after forming a complex with NDs even at a high ND concentration (10^{-8} M), which suggests it is very likely that protein could retain its biological functionality upon complexing with NDs, since its structural features are preserved to a large extent. From the second derivative spectra as shown in figure 1(b), BSA in the ND–BSA complex does not show a major decrease in its α-helix intensity (ca. 1660 cm^{-1}) upon forming a complex with NDs, which agrees well with the findings from CD spectra.

It is noteworthy that gold nanoparticles have been extensively studied in nanoparticle–biomolecule related work [39]. However, previous research [30] revealed that when gold nanoparticle concentration was increased to 1.1 nM protein

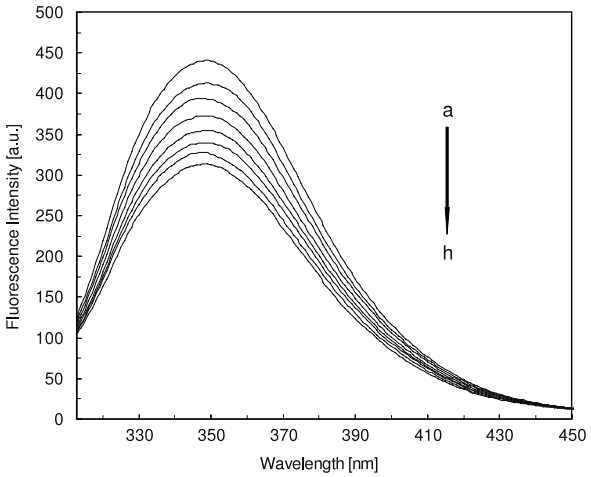

Figure 4. The fluorescence emission spectra of 1.5×10^{-6} M BSA (curve a) with the regular addition of NDs at pH 7.4. ND concentration is from 1.2×10^{-8} to 8.2×10^{-8} M (curves b–h).

BSA could only retain ca. 75% of its original structure while in the present work BSA could retain nearly 80% of its structural features even when ND concentration was increased up to 10^{-8} M, which could probably be attributed to the relatively lower binding force involved in the ND–protein than that in the gold nanoparticle–protein complex.

3.3. Fluorescence quenching studies

Fluorescence spectroscopy could provide useful information regarding the structural changes of protein [40]. Normally the interaction between a fluorophore and a molecule induces perturbation or modification in the fluorescence parameters such as intensity, peak position, etc, and these perturbations in fluorescence parameters allow information about the environment of the fluorophore to be obtained, which enables the understanding of the nature and origin of interactions between the fluorophore and other molecules [40, 41]. Tryptophan, tyrosine and phenylalanine are three intrinsic fluorophores which are responsible for the fluorescence properties of proteins. The tryptophan (Trp) fluorescence is the most sensitive to the environment change [40]. BSA in the present work is a widely used model protein [42, 43], which possesses two Trp residues [44]. By analyzing the fluorescence emission spectra of Trp in the ND–BSA complex, the BSA structural change in the region of the Trp residues can be obtained. In the present fluorescence analysis, 295 nm was used as excitation wavelength instead of 280 nm to avoid the tyrosine residue fluorescence [44, 45]. Therefore the Trp is the only fluorophore studied in the present work.

Figure 4 shows the typical fluorescence emission spectra of the BSA in the absence and presence of NDs at pH 7.4. Originally at pH 7.4 the BSA emission spectrum peaks at ca. 350 nm while with the regular addition of NDs the emission spectra undergo a considerable intensity decrease as well as a slight blue-shift in emission maximum. Obviously the fluorescence emission of Trp in BSA is quenched in the presence of NDs.

Table 1. The Stern–Volmer constant K_{SV} and the slope of the trend line in the double-wavelength method K_{slope}.

pH	K_{SV} (M^{-1})	K_{slope} (−)
3.5	$4.75 \times 10^6 \pm 0.1 \times 10^6$	$8.51 \times 10^{-3} \pm 0.68 \times 10^{-3}$
4.7	$5.5 \times 10^6 \pm 0.05 \times 10^6$	$3.16 \times 10^{-3} \pm 0.38 \times 10^{-3}$
6.0	$4.92 \times 10^6 \pm 0.1 \times 10^6$	$2.05 \times 10^{-3} \pm 0.29 \times 10^{-3}$
7.4	$4.91 \times 10^6 \pm 0.08 \times 10^6$	$4.29 \times 10^{-3} \pm 0.68 \times 10^{-3}$
9.0	$6.63 \times 10^6 \pm 0.22 \times 10^6$	$1.06 \times 10^{-2} \pm 0.24 \times 10^{-2}$

The fluorescence quenching process could be described by the Stern–Volmer equation as in equation (3) [40]:

$$\frac{F_0}{F} = 1 + k_q \tau_0 [Q] = 1 + K_{SV}[Q] \tag{3}$$

where F_0 and F are the maximum fluorescence intensities of BSA in the absence and presence of NDs, respectively while K_{SV} the Stern–Volmer constant (M^{-1}) which is a measure of quenching efficiency and Q is the quencher (ND) concentration (M). k_q and τ_0 are the bimolecular quenching constant (M^{-1} s^{-1}) and the mean fluorescence lifetime of the fluorophore in the absence of quencher (s).

If we plot $\frac{F_0}{F}$ against $[Q]$ then we have K_{SV} as the slope of the linear regression curve, which is given in table 1. According to the $\frac{F_0}{F} \sim [Q]$ curve, the Stern–Volmer constant K_{SV} is determined, which shows that all the Stern–Volmer constants are of the order of 10^6 M^{-1}. For BSA, the lifetime of fluorophore τ_0 is approximately 5×10^{-9} s [30, 46]. Then the bimolecular quenching constant k_q could be determined, from equation (3), to be of the order of 10^{14}–10^{15} M^{-1} s^{-1}, which is much higher than the maximum bimolecular quenching constant for a diffusion-controlled quenching process (ca. 10^{10} M^{-1} s^{-1}). The high k_q obtained in the quenching process suggests that there is specific strong interaction between the NDs and BSA and the dominating quenching mechanism involved is static quenching by complex formation [47, 48].

The Stern–Volmer constant K_{SV}, as given in table 1, peaks at pH 9.0 which is followed by that of pH 4.7. For pHs 3.5, 6.0, and 7.4, K_{SV} has almost the same values. To illustrate the Stern–Volmer constant changes with regard to pH, the change in the position of Trp emission maximum is studied. Protein tertiary structure is held together primarily by hydrophobic interactions. Fluorescence spectroscopy can detect the hydrophobicity of the fluorophore buried inside the hydrophobic region of protein so that the information regarding the protein tertiary structural change can be revealed. Changes in protein tertiary structure (such as unfolding) very often lead to a large change in fluorescence emission maximum. Normally, once protein undergoes unfolding, the emission maximum is red-shifted to a longer wavelength [28], which could be attributable to the exposure of fluorophore to solvent. In the present study, the blue-shift in the position of BSA emission maximum means the complexation with NDs might not perturb the BSA tertiary structure significantly, suggesting that major unfolding of BSA tertiary structure is unlikely to occur. This is consistent with some previous work dealing with fluorescence spectroscopy study on protein tertiary structure changes [49, 50].

Actually the shift in the position of the BSA emission maximum is small, as shown in figure 4. In order to determine the pH effect on the emission maximum more accurately, the double-wavelength method is employed to give quantitative evaluations as used in the previous research [51]. This method makes use of the ratio of fluorescence intensities at two wavelengths: the one on the left (F_L) and the one on the right (F_R) slope of the spectrum. The wavelengths of F_L and F_R are 20 nm away from the emission maximum of native BSA at different pHs. In this study, to make the double-wavelength method more quantitative, the slope for the trend line of the data points is used to evaluate the emission maximum shift: the greater the slope, the more the emission maximum shift. The trend lines obtained from the double-wavelength method are given in figure 5. The slope for each trend line is denoted as K_{slope} and listed in table 1, which shows noticeable blue shifts for all pHs. Sharp contrasts could be seen for emission maximum shift among different pHs with pH 9.0 the highest and pH 3.5 the second highest while for pHs 4.7, 6.0, and 7.4 the shifts are much lower. BSA undergoes conformational changes at different pHs [48, 52–54]. At pH lower than 4.3 BSA is in expanded form (E form, pH $<$ 2.7) and fast form (F form, pH 2.7–4.3) while between pH 4.3 and 8 it shifts to normal form (N form). As pH increases further, the BSA experiences basic (B form, pH 8–10) and aged forms (A form, pH $>$ 10). Among all these forms, the normal form is the most stable and compact. With pH shifting either up or down beyond normal form, the BSA undergoes structural changes becoming less stable in its structure. Because of the structural changes when BSA is in its fast and basic forms, it is relatively less compact so that the environment of the Trp residue might be relatively easily influenced by NDs which form complexes with BSA. For pHs 4.7, 6.0, and 7.4, the compact structure of BSA in normal form makes the environment of the Trp residue not as easily influenced by NDs as in the cases of pHs 3.5 and 9.0. Therefore for BSA forming complexes with NDs at pHs 3.5 and 9.0, its Trp residues are actually exposed to a more hydrophobic environment than that at pHs 4.7, 6.0, and 9.0, which could well account for the data given in figure 5 that the blue shifts for pHs 3.5 and 9.0 are much higher than those for other pHs in normal form.

With the understanding of the emission maximum shift, the fluorescence quenching results given in table 1 can be explained. At pH 9.0 the environment of the Trp residue is relatively easily altered by binding with NDs so the quenching is the most efficient. For pHs in normal form range (4.3–8), three pHs have nearly the same Stern–Volmer constants with that at pH 4.7 relatively higher than those at pHs 6.0 and 7.4. For pH 3.5, the Stern–Volmer constant is close to those in normal form but not as high as that at pH 9.0. That is probably because at pH 3.5 NDs tend to form large aggregates so that the number of BSA forming complexes with NDs is greatly reduced (figure 6). Therefore the quenching of the overall BSA fluorescence at pH 3.5 is not as efficient as at other pHs even though at pH 3.5 the environment of the Trp residue might be more easily influenced by NDs than those at pHs 4.7, 6.0, and 7.4.

According to the above spectroscopic studies, it is reasonable to believe that NDs could provide sufficient affinity with protein for its immobilization and at the same time the binding force falls in an acceptable range in terms of preserving protein structural features. Actually there needs to be a trade-off between nanoparticle–biomolecule binding force and biomolecule structural integrity. On the one hand,

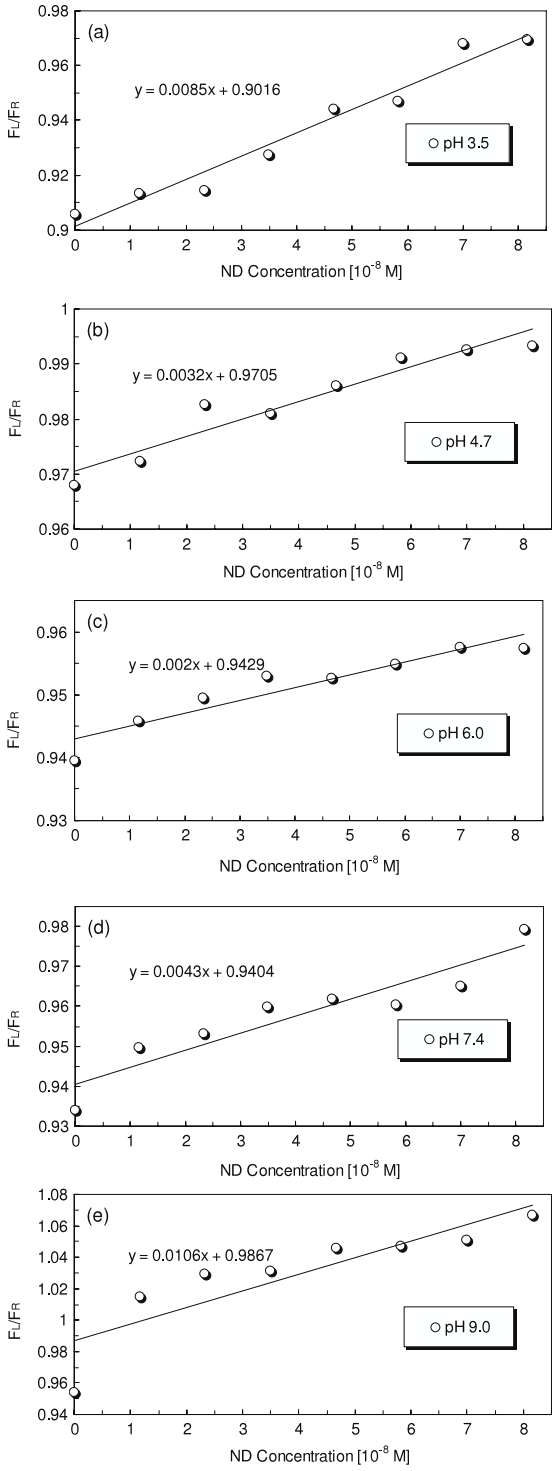

Figure 5. The influence of ND–BSA interaction on the position of the emission maximum of BSA determined by the ratio of fluorescence intensities at two wavelengths: on the left (F_L) and on the right (F_R) slopes of the spectrum (20 nm away from the emission maximum) at different pHs.

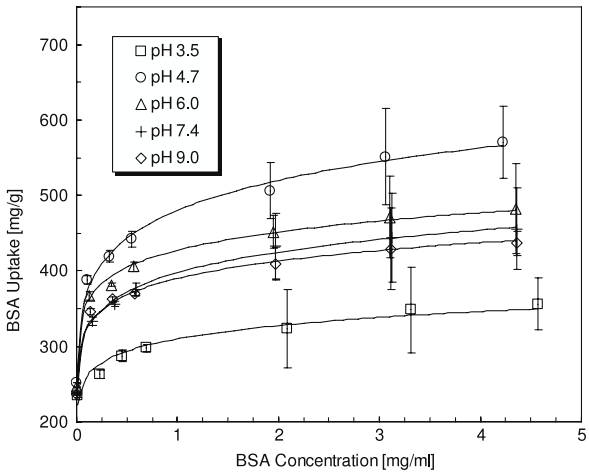

Figure 6. Adsorption isotherms of BSA onto NDs at different pHs. The solid curves are the best fits of the experimental data to the Freundlich adsorption model (equation (4)). The error bar represents standard deviation.

nanoparticles are expected to have high binding force with biomolecules; on the other hand, too strong a binding force would definitely disrupt the biomolecule structural features.

The retention of original structure of proteins (albumin, lysozyme, etc) in the nanoparticle–protein complex could possibly be attributable to the high curvature of nanoparticles (NDs in the present work), which has been evidenced by some previous research [23, 55]. The NDs in the present work have a single crystal size of ca. 5 nm. Thus the ND aggregates consisting of nanodiamond crystals would exhibit very high local curvature, facilitating the retention of albumin structural features. In addition, some previous research devoted to biosensor applications using NDs has already demonstrated that NDs could preserve the biological functionality of biomolecules immobilized on their surface to a large extent, such as α-bungarotoxin (α-BTX) and lysozyme [17, 56].

3.4. Equilibrium adsorption of BSA

BSA adsorption behavior on the ND surface was studied by adsorption isotherms at different pHs. As can be seen from figure 6, most adsorption isotherms for BSA onto the ND surface show a steep slope at low BSA concentrations, suggesting a strong interaction between NDs and BSA. Obviously NDs have the highest BSA uptake at the isoelectric point (pI) of BSA (ca. pH 4.7) and the lowest at pH 3.5. For each isotherm, the BSA uptakes of the last two points only differ by less than 5%, so it might be reasonable to conclude that the adsorption reaches saturation at high concentration range under the current adsorption conditions. Based on this fact, the maximum BSA uptake q_m is determined as the average of the last two BSA uptakes on each isotherm, and is listed in table 2. As shown in table 2, the maximum saturated BSA uptake is ca. 560.5 mg g^{-1}, which is obtained at pH 4.7. According to the data given by the manufacturer, the surface area of the NDs is ca. 300 m^2 g^{-1}. Combining these

Table 2. Maximum BSA uptake q_m, Freundlich constant K_f, and the affinity of NDs to BSA $1/n$.

pH	q_m (mg g^{-1})	K_f (−)	$1/n$ (−)
3.5	352.1 ± 5.7	310.1 ± 3.8	$7.92 \times 10^{-2} \pm 0.78 \times 10^{-2}$
4.7	560.5 ± 13.3	480.2 ± 4.0	$1.15 \times 10^{-1} \pm 0.05 \times 10^{-1}$
6.0	476.7 ± 8.1	427.4 ± 2.5	$7.91 \times 10^{-2} \pm 0.29 \times 10^{-2}$
7.4	449.9 ± 8.1	397.9 ± 2.1	$9.51 \times 10^{-2} \pm 0.3 \times 10^{-2}$
9.0	432.7 ± 5.4	390.1 ± 3.5	$8.23 \times 10^{-2} \pm 0.49 \times 10^{-2}$

two gives a BSA adsorption density of 1.9 mg m^{-2} (1.7×10^{16} BSA molecules m^{-2}, considering that the BSA molecular weight is ca. 67 000 Da [57]) for BSA adsorbed on the ND surface at saturation. It is known that BSA has geometric dimensions of $9.5 \times 5.0 \times 5.0$ nm^3 [57]. Therefore for BSA adsorption onto a surface there are two possibilities: a 'side-on' adsorption mode with an adsorption area of 9.5×5.0 nm^2 and an 'end-on' adsorption mode with an adsorption area of 5.0×5.0 nm^2 [58]. The BSA adsorption density required for an adsorption monolayer on the ND surface is determined as 1.9×10^{16} BSA molecules m^{-2} for the side-on mode and 3.31×10^{16} BSA molecules m^{-2} for the end-on mode, which corresponds to 2.1 mg m^{-2} and 3.6 mg m^{-2} for the side-on and end-on modes, respectively. The actual maximum BSA adsorption density in the present work is 1.9 mg m^{-2} which is very close to the minimum BSA density required for a side-on monolayer. The proposed 'side-on/end-on' adsorption mode is based on the ideal situation where no change occurs in terms of protein structural features, so it cannot be exactly accurate since protein is always subjected to structural changes once adsorbed onto a surface. However, the spectroscopic studies in the present work have proved that most of the BSA structural features are preserved upon being attached to the ND surface, which means the BSA structural change is not significant. In addition, BSA is prone to being adsorbed in a side-on fashion to cover the whole nanoparticle surface according to previous research [58]. Therefore the use of the side-on mode to determine the density of adsorbed BSA on a nanoparticle surface could be a close approximation, as demonstrated by the BSA adsorption data in the present research.

It is found that the Langmuir model cannot fit the adsorption data. This might be attributable to the interaction (such as steric hindrance) among adsorbed BSA molecules on the ND surface, considering the relative large molecular size of BSA. In addition, the ND surface might not be ideally uniform.

The Freundlich model can provide a desirable fit for the adsorption data, as shown in figure 6. The Freundlich model is given in equation (4):

$$q_e = K_f C_e^{(1/n)} \tag{4}$$

where q_e and C_e are equilibrium BSA concentration on the ND surface (mg g^{-1}) and in the solution (mg ml^{-1}), respectively. K_f is the Freundlich constant related to the binding capacity of NDs for BSA and $1/n$ is the affinity of NDs to BSA [59]. K_f and $1/n$ are determined by nonlinear regression of equation (4).

K_f and $1/n$ are summarized in table 2. Both K_f and $1/n$ show similar strong pH dependence to q_m, reaching their

maximum at the pI of BSA and approaching their minimum at pHs 3.5 and 6.0.

The ND surface used in the present research mainly contains carboxyl and hydroxyl groups, as demonstrated in our previous work [60]. According to the zeta-potential measurements as shown in figure 7, the ND surface is always negatively charged over the whole pH range under investigation while BSA shows an isoelectric point (pI) at pH 4.6. These results agree well with previous reports [58, 61]. As shown in figure 7, the zeta-potential of the NDs decreases with the decrease of pH, which might result from the protonation of negatively charged groups on the ND surface. The interaction between protein and surface includes hydrophobic interaction, ionic interaction, hydrogen boding, and van der Waals interaction [61, 62]. The van der Waals force is usually negligible in comparison with other forces, as detailed in the previous research [62]. If electrostatic interaction is dominant in the ND–BSA interaction, the highest BSA uptake would be at pH 3.5. That is because only at pH 3.5 does BSA have an electrostatic attraction with ND. The fact that the BSA uptake at pH 3.5 is the lowest suggests that the electrostatic interaction would not be the dominating force. It is known that the nanodiamond surface is covered by a thin layer of graphite [8], which is hydrophobic in nature. Due to the hydrophobic nature on the nanodiamond surface, the hydrophobic force tends to dominate the BSA adsorption process, especially when the BSA molecule contains less or no surface charge. Previous research [62] revealed that for a surface containing a low density of carboxyl groups the hydrophobic force is dominant in the protein adsorption process, which is pH sensitive, while for the surface high in carboxyl density the hydrogen bond dominates. Dynamic light scattering measurements show that NDs exist in the form of aggregates ranging from ca. 300 to 680 nm in size as the pH changes from ca. 9.0 to 3.5 (data not shown), suggesting that the carboxyl density on the ND surface is relatively low. Actually for a zeta-potential with absolute value lower than 30 mV, the crystals might tend to form aggregates because of the relatively low surface charge [63], which is the case in the present work. Because of the hydrophobic nature of the ND surface graphite layer and the relatively low ND surface charge, hydrophobic force tends to dominate the BSA adsorption process. Accordingly, the BSA uptake and the ND–BSA affinity peak approximately at the pI of BSA.

At pH 3.5 the ND has the lowest BSA uptake and lowest affinity with BSA. This could be attributable partly to the fact that hydrophobic force dominates the ND–BSA interaction and partly to the relatively larger size of ND aggregates at low pH. The size of ND aggregates is kept at ca. 300 nm in the pH range of 6–8.5, while it increases sharply to nearly 680 nm as the pH is reduced to ca. 3.5 (data not shown). The relatively larger particle size of ND aggregates at low pH would reduce the actual surface area available for the BSA adsorption, and thus reduce the BSA uptake and ND–BSA affinity.

Due to low surface charge and high surface energy, the NDs in the solution are in the form of aggregates rather than single crystals. Therefore the BSA adsorption behavior on NDs is more dependent on the properties of ND aggregates.

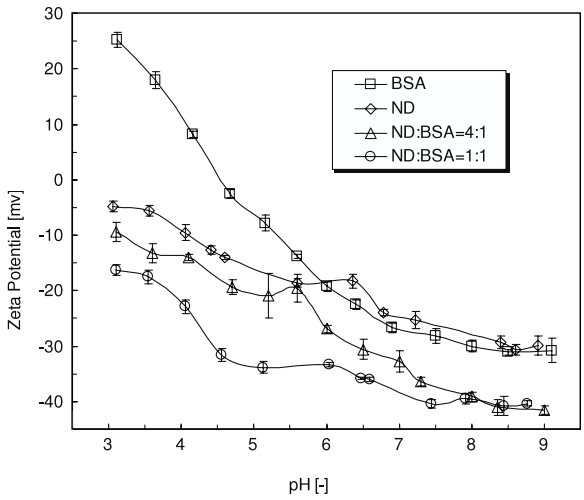

Figure 7. The zeta potentials of native BSA, ND, and the ND–BSA complex (with ND:BSA mass ratio of 4:1 and 1:1) over the pH range of 3–9. The error bar represents standard deviation.

However, the surface properties of ND single crystal (such as surface hydrophobicity and charge) actually affect BSA adsorption behavior indirectly since ND aggregate is composed of single ND crystals.

It is interesting to find that, as shown in figure 7, by adding BSA to ND suspension (ND:BSA = 4:1, mass ratio) the zeta-potential is decreased to a lower level in comparison with either ND or native BSA. A further addition of BSA brings the zeta-potential even lower (ND:BSA = 1:1, mass ratio). The addition of BSA into ND suspension gives rise to the formation of ND–BSA complexes by virtue of the high affinity of NDs with BSA. For the conformation of ND–BSA complexes, it is possible that BSA is attached on the surface of ND aggregates, but there must be other forms of ND–BSA complex because if BSA only exists on the ND surface the zeta-potential of the ND–BSA complex should be residing between those of the ND and BSA instead of decreasing to a lower level as shown in figure 7. According to the previous research, proteins such as BSA could facilitate the dispersion of carbon nanotubes (CNTs) at the individual nanotube level by a protein-assisted CNT exfoliation process [64–66]. The CNT aggregates were debundled in the presence of BSA so that the CNTs could be well dispersed in solution. In view of the role that BSA plays in CNT dispersion, it is very likely that after attaching to BSA the strong binding force between NDs and BSA might result in partial breakup of ND aggregates into relatively small ND–BSA aggregates. In the case that the ND aggregates break up into relatively small ND–BSA aggregates, more negative surface charge of the ND might be exposed to the solution, which then becomes 'surface charged'. The zeta-potential measurement is performed by measuring the electrophoretic velocity of the nanoparticles in the solution. For ND aggregate, by binding with BSA to form relatively small ND–BSA aggregates, more negative surface charge exposition to the solution might be able to enhance the electrophoretic velocity of the ND–BSA complex as compared with single ND aggregate. Therefore the zeta-potential of the ND–BSA is more negative.

4. Conclusion

In this study, the conformation of BSA in the ND–BSA complex was investigated by a series of characterization techniques. Fourier transform infrared spectroscopy shows an evident change in BSA secondary structure upon binding with NDs. The UV–vis and CD spectroscopies further indicate that most BSA structural features could be preserved in the ND–BSA complex. The fluorescence spectroscopy reveals that Trp residues in BSA are placed in a more hydrophobic environment in the ND–BSA complex suggesting that major protein unfolding is unlikely to occur. For the adsorption isotherms obtained at different pHs (3.5, 4.7, 6.0, 7.4, 9.0), both BSA uptake and the affinity between NDs and BSA peak at pH 4.7, which suggests that hydrophobic force dominates the BSA adsorption process. The adsorption isotherms can be well fitted by the Freundlich but not the Langmuir model. The zeta-potential measurements further suggest that after binding with BSA, the strong binding force between NDs and BSA might result in partial breakup of ND aggregates into relatively small ND–BSA aggregates. The results obtained have demonstrated that NDs are able to preserve the albumin structural features to a large extent in the ND–albumin complex and are very promising to be used for biosensor applications.

Acknowledgments

The present work is financially supported by the Natural Sciences and Engineering Research Council of Canada, the Canada Research Chair Program, and the Canada Foundation for Innovation grant. We also appreciate the cordial assistance from Mr Jagbir Singh, from the College of Pharmacy and Nutrition at the University of Saskatchewan, in zeta-potential measurement.

References

[1] Daniel M C and Astruc D 2004 *Chem. Rev.* **104** 293–346
[2] Panyam J and Labhasetwar V 2003 *Adv. Drug Deliv. Rev.* **55** 329–47
[3] Medintz I L, Uyeda H T, Goldman E R and Mattoussi H 2005 *Nat. Mater.* **4** 435–46
[4] Katz E and Willner I 2004 *Angew. Chem. Int. Edn* **43** 6042–108
[5] Krueger A 2008 *Chem.—Eur. J.* **14** 1382–90
[6] Shenderova O A, Zhirnov V V and Brenner D W 2002 *Crit. Rev. Solid State Mater. Sci.* **27** 227–356
[7] Huang H J, Dai L M, Wang D H, Tan L S and Osawa E 2008 *J. Mater. Chem.* **18** 1347–52
[8] Krueger A 2008 *Adv. Mater.* **20** 2445–9
[9] Puzyr A P, Baron A V, Purtov K V, Bortnikov E V, Skobelev N N, Moginaya O A and Bondar V S 2007 *Diamond Relat. Mater.* **16** 2124–8
[10] Schrand A M, Huang H J, Carlson C, Schlager J J, Osawa E, Hussain S M and Dai L M 2007 *J. Phys. Chem.* B **111** 2–7
[11] Warheit D B 2006 *Carbon* **44** 1064–9
[12] Kong X L, Huang L C L, Hsu C M, Chen W H, Han C C and Chang H C 2005 *Anal. Chem.* **77** 259–65
[13] Huang L C L and Chang H C 2004 *Langmuir* **20** 5879–84
[14] Huang H J, Pierstorff E, Osawa E and Ho D 2008 *ACS Nano* **2** 203–12
[15] Steinmuller-Nethl D *et al* 2006 *Biomaterials* **27** 4547–56
[16] Bondar' V S, Pozdnyakova I O and Puzyr' A P 2004 *Phys. Solid State* **46** 758–60
[17] Nguyen T T B, Chang H C and Wu V W K 2007 *Diamond Relat. Mater.* **16** 872–6
[18] Chung P H, Perevedentseva E, Tu J S, Chang C C and Cheng C L 2006 *Diamond Relat. Mater.* **15** 622–5
[19] Huang T S, Tzeng Y, Liu Y K, Chen Y K, Walker K R, Guntupalli R and Liu C 2004 *Diamond Relat. Mater.* **13** 1098–102
[20] Kong X L, Huang L C L, Liau S C V, Han C C and Chang H C 2005 *Anal. Chem.* **77** 4273–7
[21] Lundqvist M, Sethson I and Jonsson B H 2004 *Langmuir* **20** 10639–47
[22] Jiang X, Jiang U G, Jin Y D, Wang E K and Dong S J 2005 *Biomacromolecules* **6** 46–53
[23] Roach P, Farrar D and Perry C C 2006 *J. Am. Chem. Soc.* **128** 3939–45
[24] Nakanishi K, Sakiyama T and Imamura K 2001 *J. Biosci. Bioeng.* **91** 233–44
[25] Karajanagi S S, Vertegel A A, Kane R S and Dordick J S 2004 *Langmuir* **20** 11594–9
[26] Forato L A, Bernardes R and Colnago L A 1998 *Anal. Biochem.* **259** 136–41
[27] Souillac P O, Middaugh C R and Rytting J H 2002 *Int. J. Pharm.* **235** 207–18
[28] Creighton T E 1997 *Protein Structure: A Practical Approach* 2nd edn (Oxford: Oxford University Press)
[29] Wang Y S, Jiang Q, Liu L R and Zhang Q Q 2007 *Polymer* **48** 4135–42
[30] Shang L, Wang Y Z, Jiang J G and Dong S J 2007 *Langmuir* **23** 2714–21
[31] Buijs J, Norde W and Lichtenbelt J W T 1996 *Langmuir* **12** 1605–13
[32] Jackson M and Mantsch H H 1995 *Crit. Rev. Biochem. Mol. Biol.* **30** 95–120
[33] Vass E, Hollosi M, Besson F and Buchet R 2003 *Chem. Rev.* **103** 1917–54
[34] Roach P, Farrar D and Perry C C 2005 *J. Am. Chem. Soc.* **127** 8168–73
[35] Giacomelli C E, Bremer M G E G and Norde W 1999 *J. Colloid Interface Sci.* **220** 13–23
[36] Dong A, Huang P and Caughey W S 1992 *Biochemistry* **31** 182–9
[37] Kanakis C D, Tarantilis P A, Polissiou M G, Diamantoglou S and Tajmir-Riahi H A 2006 *J. Mol. Struct.* **798** 69–74
[38] Pi Y Y, Shang Y Z, Peng C J, Liu H L, Hu Y and and Jiang J W 2006 *Biopolymers* **83** 243–9
[39] Panyala N R, Pena-Mendez E M and Havel J 2009 *J. Appl. Biomed.* **7** 75–91
[40] Albani J R 2004 *Structure and Dynamics of Macromolecules: Absorption and Fluorescence Studies* (Amsterdam: Elsevier) pp 141–92
[41] Royer C A 2006 *Chem. Rev.* **106** 1769–84
[42] Yang Y Y, Chung T S and Ng N P 2001 *Biomaterials* **22** 231–41
[43] Mellott M B, Searcy K and Pishko M V 2001 *Biomaterials* **22** 929–41
[44] Sulkowska A 2002 *J. Mol. Struct.* **614** 227–32
[45] Albani J R 2004 *Structure and Dynamics of Macromolecules: Absorption and Fluorescence Studies* (Amsterdam: Elsevier) pp 99–140
[46] Wei Y L, Li J Q, Dong C, Shuang S M, Liu D S and Huie C W 2006 *Talanta* **70** 377–82
[47] Qin C, Xie M X and Liu Y 2007 *Biomacromolecules* **8** 2182–9

[48] Papadopoulou A, Green R J and Frazier R A 2005 *J. Agric. Food Chem.* **53** 158–63
[49] Creamer L K 1995 *Biochemistry* **34** 7170–6
[50] Saha B and Das G 2009 *J. Phys. Chem.* C **113** 15667–75
[51] Klajnert B, Stanislawska L, Bryszewska M and Palecz B 2003 *Biochim. Biophys. Acta Proteins Proteomics* **1648** 115–26
[52] Lee C T, Smith K A and Hatton T A 2005 *Biochemistry* **44** 524–36
[53] Sadler P J and Tucker A 1993 *Eur. J. Biochem.* **212** 811–7
[54] Efimova Y M, Haemers S, Wierczinski B, Norde W and van Well A A 2007 *Biopolymers* **85** 264–73
[55] Vertegel A A, Siegel R W and Dordick J S 2004 *Langmuir* **20** 6800–7
[56] Liu K K, Chen F, Chen P Y, Lee T J F, Cheng C L, Chang C C, Ho Y P and Chao J I 2008 *Nanotechnology* **19** 205102
[57] Jachimska B, Wasilewska M and Adamczyk Z 2008 *Langmuir* **24** 6866–72
[58] Rezwan K, Meier L P, Rezwan M, Voros J, Textor M and Gauckler L J 2004 *Langmuir* **20** 10055–61
[59] Labhasetwar V, Song C X, Humphrey W, Shebuski R and Levy R J 1998 *J. Pharm. Sci.* **87** 1229–34
[60] Wang H D, Yang Q Q and Niu C H 2010 *Diamond Relat. Mater.* **19** 441–4
[61] Brewer S H, Glomm W R, Johnson M C, Knag M K and Franzen S 2005 *Langmuir* **21** 9303–7
[62] Yoon J Y, Park H Y, Kim J H and Kim W S 1996 *J. Colloid Interface Sci.* **177** 613–20
[63] Freitas C and Muller R H 1998 *Int. J. Pharm.* **168** 221–9
[64] Karajanagi S S, Yang H C, Asuri P, Sellitto E, Dordick J S and Kane R S 2006 *Langmuir* **22** 1392–5
[65] Edri E and Regev O 2008 *Anal. Chem.* **80** 4049–54
[66] Edri E and Regev O 2009 *Langmuir* **25** 10459–65